Available online at www.sciencedirect.com
ScienceDirect
Remote Sensing of Environment 104 (2006) 133 – 146
Remote Sensing of Environment
www.elsevier.com/locate/rse

Remote sensing image-based analysis of the relationship between urban heat island and land use/cover changes

Xiao-Ling Chen [a], Hong-Mei Zhao [a,*], Ping-Xiang Li [a], Zhi-Yong Yin [b]

[a] State Key Laboratory of Information Engineering in Surveying, Mapping and Remote Sensing (LIESMARS), Wuhan University, 430079 P.R.China
[b] Marine Science and Environmental Studies, University of San Diego, San Diego, CA 92110, USA

Received 16 February 2005; received in revised form 9 November 2005; accepted 10 November 2005

Abstract

Global warming has obtained more and more attention because the global mean surface temperature has increased since the late 19th century. As more than 50% of the human population lives in cities, urbanization has become an important contributor for global warming. Pearl River Delta (PRD) in Guangdong Province, southern China, is one of the regions experiencing rapid urbanization that has resulted in remarkable Urban Heat Island (UHI) effect, which will be sure to influence the regional climate, environment, and socio-economic development. In this study, Landsat TM and ETM+ images from 1990 to 2000 in the PRD were selected to retrieve the brightness temperatures and land use/cover types. A new index, Normalized Difference Bareness Index (NDBaI), was proposed to extract bare land from the satellite images. Additionally, Shenzhen, which has experienced the fastest urbanization in Guangdong Province, was taken as an example to analyze the temperature distribution and changes within a large city as its size expanded in the past decade. Results show that the UHI effect has become more prominent in areas of rapid urbanization in the PRD region. The spatial distribution of heat islands has been changed from a mixed pattern, where bare land, semi-bare land and land under development were warmer than other surface types, to extensive UHI. Our analysis showed that higher temperature in the UHI was located with a scattered pattern, which was related to certain land-cover types. In order to analyze the relationship between UHI and land-cover changes, this study attempted to employ a quantitative approach in exploring the relationship between temperature and several indices, including the Normalized Difference Vegetation Index (NDVI), Normalized Difference Water Index (NDWI), Normalized Difference Bareness Index (NDBaI) and Normalized Difference Build-up Index (NDBI). It was found that correlations between NDVI, NDWI, NDBaI and temperature are negative when NDVI is limited in range, but positive correlation is shown between NDBI and temperature.

Keywords: Land use/cover change (LUCC); Urban heat island (UHI); NDWI, NDVI, NDBI and NDBaI; PRD; Vegetation water content (VWC)

1. Introduction

Urban heat island (UHI) has long been a concern for more than 40 years. One of the earliest UHI studies was conducted in 1964 (Nieuwolt, 1966) in the urban southern Singapore. Extensive urbanized surfaces modify the energy and water balance processes and influence the dynamics of air movement (Oke, 1987). The characteristics of the UHI effect have been studied extensively. For example, Deosthali (2000) found that at night, the core of the city appeared as both heat and moisture islands whereas at the time of sunrise as heat and dry islands. The average maximum UHI is weakest in summer and strong in autumn and winter (Kim & Baik, 2002; Zhong, 1996). The UHI intensity was found to be inversely correlated with the rural temperature, while the spatial extent was found to be independent of both heat island magnitude and rural temperature (Streutker, 2002). Giridharan et al. (2004) studied the daytime UHI effect in high-rise and high-density residential developments in Hong Kong, and the results showed that energy efficient designs could be achieved by manipulating surface albedo, sky view factor and total height to floor area ratio while maximizing cross ventilation. Saaroni et al. (2000) adopted a new combined method of monitoring the UHI from different levels and on different scales, which enabled a spatial assessment of the city's UHI and its diverse thermal coverage characteristics.

* Corresponding author. Tel.: +86 27 6248 1762, +86 27 6877 8092; fax: +86 27 6877 8229, +86 27 6877 8969.
E-mail addresses: zhm8012@tom.com, cecxl@yahoo.com (H.-M. Zhao).

0034-4257/$ - see front matter © 2006 Elsevier Inc. All rights reserved.
doi:10.1016/j.rse.2005.11.016

Rao (1972) was the first to demonstrate that urban areas could be identified from the analyses of thermal infrared data acquired by a satellite. Gallo et al. (1995) reviewed and represented a satellite perspective on the assessment of UHI. Studies on the UHI phenomenon using satellite derived land surface temperature (LST) measurements have been conducted primarily using NOAA AVHRR data (Gallo & Owen, 1998a,b; Streutker, 2002, 2003) for regional-scale urban temperature mapping. Recently, Landsat Thermatic Mapper (TM) and Enhanced Thermatic Mapper Plus (ETM+) thermal infrared (TIR) data with 120 m and 60 m spatial resolutions, respectively, have also been utilized for local-scale studies of UHI (Chen, Wang, & Li, 2002; Weng, 2001). Research on LST showed that the partitioning of sensible and latent heat fluxes and thus surface radiant temperature response was a function of varying surface soil water content and vegetation cover (Owen et al., 1998). This finding encourages research on the relationship between LST and vegetation abundance (e.g. Gallo & Owen, 1998a,b; Weng, 2001; Weng et al., 2003).

UHI intensity is related to patterns of land use/cover changes (LUCC), e.g. the composition of vegetation, water and built-up and their changes. Hawkins et al. (2004) studied the effect of rural variability in calculating the urban heat island effect. Qualitative studies on the relationship between land use/cover pattern (LUCP) and LST will help us in land use planning. It is known that various vegetation indices obtained from remote sensing images can be used in the assessment of vegetation cover qualitatively and quantitatively (Tian & Xiangjun, 1998). Relationships between various vegetation indices and percent vegetation cover have been established by using regression analysis (Purevdorj, Tateishi, Ishiyama, & Honda, 1998), such as Ratio Vegetation Index (RVI), Normalized Difference Vegetation Index (NDVI), Difference Vegetation Index (DVI) and Perpendicular Vegetation Index (PVI). The NDVI has been used for the estimation of vegetation productivity and rainfall in semiarid areas (Chen et al., 2004; Wang et al., 2004), while the Normalized Difference Water Index (NDWI) can be used for the determination of vegetation water content (VWC) based on physical principles (Gao, 1996). Although NDVI has limited capability for estimating VWC (Ceccato et al., 2002), it is ideal to integrate NDVI and NDWI to represent the state of vegetation. Zha, Gao, and Ni (2003) developed the Normalized Difference Built-up Index (NDBI) to identify urban and built-up areas. It is possible that the utilization of NDVI, NDWI and NDBI could represent land-cover types quantitatively so that the relationships between different indices, such as NDVI, NDWI, NDBI, and temperature can be established in UHI studies.

The purpose of our study is to examine the changes in land use/cover pattern in a rapidly changing area of the PRD region in relation to urbanization since the 1990s and then to investigate the impact of such changes on the intensity and spatial pattern of the UHI effect in the region. We used NDVI, NDWI and NDBI indices to extract land use/cover information from remote sensing images of different time periods and then analyzed the surface temperature retrieved from the thermal infrared band. The specific objectives of this research are: (1) to derive brightness temperature from the Landsat TM/ETM+ thermal band for the period 1990–2000; (2) to examine the spatial pattern of the land use/cover index values and their changes over the study period; (3) to investigate the relationship between brightness temperature and land use/cover pattern (LUCP) in the PRD region and the city of Shenzhen

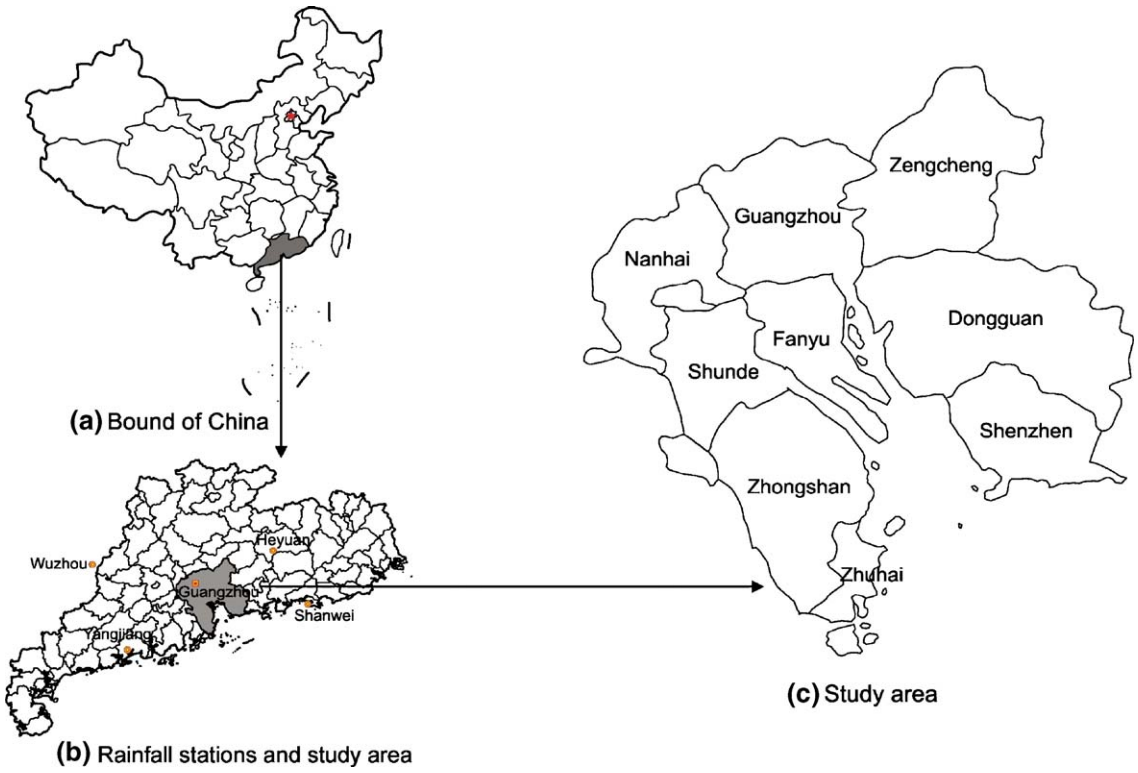

Fig. 1. Location of the Pearl River Delta and rainfall stations nearby.

in southern China; and (4) to quantitatively study the relationship between the intensity of UHI and LUP and how it has changed over time.

2. Data and methods

2.1. Study area and data

The Pearl River Delta (PRD), along the coast of South China Sea, has been selected as the study area considering its rapid urbanization in the past 25 years. Nineteen counties and cities in the PRD region were included in this study, and 9 of them are along the Pearl River estuary. This region was among the first to be open to the outside world when China started the economic reform and has experienced rapid urbanization since the 1980s, especially during the 1990s (Fig. 1). The city of Shenzhen is located between 113°46′–114°37′E and 22°27′–22°52′N (Fig. 1) which was chosen as a case study area because since 1978 it has transformed from an unknown fishing village to a city of multi-million population and a major industrial centre in southern China. Its core area, the Special Economic Zone of Shenzhen, consists of four districts, Luohu, Futian, Nanshan, and Yantian.

To quantitatively measure land surface temperature and compare urban heat island intensity in the study area, Landsat 5 TM images (Oct. 13, 1990; Oct. 29, 1994; Mar. 3, 1996 and Dec. 22, 1998) and Landsat 7 ETM+ images (Sept. 14, 2000 and Nov. 1, 2000) were selected. All images bands 1–5 and 7 have a spatial resolution of 30 m, and the thermal infrared band (band6) has a spatial resolution of 120 m for Landsat 5 TM images and 60 m for Landsat 7 ETM+ images.

In addition, an IKONOS 2000 image with a spatial resolution of 4 m, which has been rectified to the Universal Transverse Mercator (UTM) coordinate system, and a digital topographic map with a scale of 1:10000 for the city of Shenzhen were used to obtain a detailed land use/cover classification achieved by high spatial resolution.

2.2. Image pre-processing

Noise reduction is necessary for remotely sensed images, especially for the thermal infrared (TIR) band. The noise may affect the retrieval of brightness temperature or LST. There is periodic noise (e.g., stripes in the TM/band6) and non-periodic noise (e.g., speckles). In this study, a self-adaptive filter method was used to remove non-periodic noise and the Fast Fourier Transform (FFT) method was used to automatically remove periodic noise. Both the removal of periodic and non-periodic method was performed by using software ERDAS Image v8.6. Fig. 2 showed that the increase or decrease in the digital numbers (DNs) was more than 5% caused by periodic noise for the ETM+/TIR band on Nov. 1, 2000.

To analyze the changes in temperature and LUCP in the study region, multi-temporal images must be co-registered in the same coordinate system (e.g., UTM/WGS84). In this study, the raw images were geo-referenced to a common UTM coordinate system based on the hi-resolution IKONOS image and the 1:10,000 scale topographic maps, and re-sampled using the nearest neighbor algorithm with a pixel size of 30 m by 30 m for all bands, including the thermal band. The RMSE of rectification was less than 0.5 in this study.

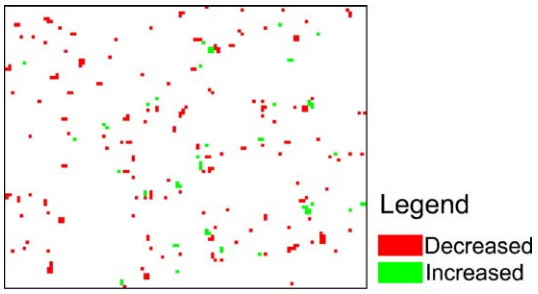

Fig. 2. Effect of periodic noise.

2.3. Derivation of brightness temperature

Satellite TIR sensors measure radiances at the top of the atmosphere (TOA), from which brightness temperatures (also known as blackbody temperatures) can be derived by using Plank's law (Dash et al., 2002). It is assumed that the water vapor content of the atmosphere is constant for a relatively small region, so that the atmospheric condition could be considered as uniform, and the influence of atmosphere on radiance temperature could be neglected. Therefore, the at-satellite brightness temperature can be used to reflect the distribution of the surface temperature fields. It is recognized that the water vapor content does vary over time due to seasonality and inter-annual variability of the atmospheric conditions. It is not appropriate to directly compare temperature represented by the at-satellite brightness temperature between multiple time periods. Therefore, we focused on the UHI intensity and its spatial patterns across the study region on the image acquisition dates. UHI intensity is measured as the difference between the peak temperature found inside the urban area and the background rural temperature (Oke, 1987). In this way, the UHI effect can be measured for the individual thermal images and then compared between different time periods. The retrieval methods of brightness temperature from the TM and ETM+ images are different, which are discussed as follows.

2.3.1. Retrieval of brightness temperature from the Landsat 5 TM images

Chen et al. (2002) proposed a method of deriving brightness temperature in two steps:

First, the digital numbers (DNs) of band6 are converted to radiation luminance (R_{TM6}, mW $cm^{-2}sr^{-1}$) by the following formula:

$$R_{TM6} = \frac{V}{255}(R_{max} - R_{min}) + R_{min} \quad (1)$$

where: V represents the DN of band6, and

$$R_{max} = 1.896(mW*cm^{-2}*sr^{-1}),$$
$$R_{min} = 0.1534(mW*cm^{-2}*sr^{-1})$$

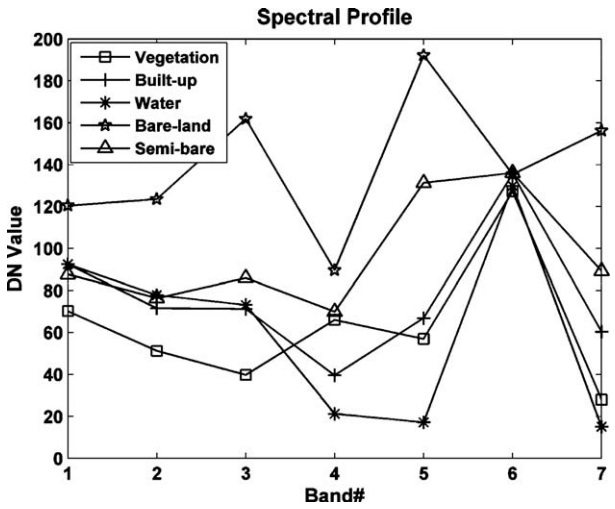

Fig. 3. Spectral profiles of five typical land use/cover types in the study area.

Then radiation luminance is converted to at-satellite brightness temperature in Kelvin, $T(K)$, by the following equation:

$$T = \frac{K1}{\ln(K2/(R_{TM6}/b)+1)} \quad (2)$$

where, $K1 = 1260.56$ K and $K2 = 60.766(\mathrm{mW} * \mathrm{cm}^{-2} * \mathrm{sr}^{-1}\ \mu\mathrm{m}^{-1})$, which are pre-launch calibration constants; b represents effective spectral range, when the sensor's response is much more than 50%, $b = 1.239(\mu m)$.

2.3.2. Retrieval of brightness temperature from the Landsat 7 ETM+ images

The Landsat 7 ETM+ 1G products were utilized for retrieving temperature in 2000. The approach to the retrieval of temperature was described in the Landsat 7 User's Handbook. It is also simplified to two separate steps as follows:

First, the DNs of band6 were converted to radiance by the following formula:

$$\text{Radiance} = \text{gain}*\text{DN} + \text{offset}; \quad (3)$$

which can also be expressed as:

$$\text{Radiance} = \frac{\text{LMAX}-\text{LMIN}}{\text{QCALMAX}-\text{QCALMIN}} *(\text{QCAL}-\text{QCALMIN}) + \text{LMIN} \quad (4)$$

where, the gain and offset can be obtained from the header file of the images, QCALMIN = 1, QCALMAX = 255, QCAL = DN, and LMAX and LMIN (also given in the header file of the images) are the spectral radiances for band6 at digital numbers 1 and 255 (i.e., QCALMIN and QCALMAX), respectively.

Then the effective at-satellite temperature of the viewed Earth-atmosphere system under the assumption of a uniform emissivity could be obtained from the above spectral radiance by the following equation:

$$T = \frac{K2}{\ln(K1/L_\lambda + 1)} \quad (5)$$

Where, T is the effective at-satellite brightness temperature in Kelvin; $K1 = 666.09$(watts/(meter squared * ster * μm)) and $K2 = 1282.71$(Kelvin) are calibration constants; and L_λ is the spectral radiance in watts/(meter squared * ster * μm).

Table 1
Indices value ranges for different land use/cover types

	NDVI	NDWI	NDBI	NDBaI
Built-up	<0.2	<0	0.10–0.30	<−0.2
Bare land	<0.2	<0	>0.25	>0
Vegetation	>0.2	>0.05	<0	<−0.25
Water	<0	>0	<0	<−0.65
Semi-bare land	>0.2	<0	>0.25	−0.1–0

2.4. Derivation of NDVI, NDWI, NDBI and NDBaI from Landsat TM and ETM+ imagery

THE NDVI, NDWI (Gao, 1996), NDBI (Zha et al., 2003) and NDBaI indices were used to characterize the land use/cover types in the study region and to study the relationships between land use/cover types and UHI quantitatively. NDVI in Eq. (6) was generally used to express the density of vegetation (Purevdorj et al., 1998).

$$\text{NDVI} = (\rho(\text{band4}) - \rho(\text{band3}))/(\rho(\text{band4}) + \rho(\text{band3})) \quad (6)$$

NDWI in Eq. (7) is a Normalized Difference Water Index, also called leaf area water-absent index, which implied the water content within vegetation (Gao, 1996; Jackson et al., 2004; Zarco-Tejada et al., 2003; Maki, Ishiahra, & Tamuva, 2004) and water state of vegetation (Maki et al., 2004). In Soil Moisture Experiments in 2002 (SMEX02), NDWI was used to evaluate the water content of vegetation for the research of arid

Table 2
Accuracy evaluation of classification in the PRD region

Class name	Reference totals	Classified totals	Number correct	Producers accuracy	Users accuracy
Bare land	26	27	27	100%	96.30%
Water	62	59	59	95.16%	100%
Fish pond	59	61	58	98.31%	95.08%
Semi-bare	76	68	64	84.21%	94.12%
Built-up	50	54	47	94%	87.04%
Forest	59	67	56	94.92%	83.58%
Cropland	114	112	103	90.35%	91.96%

Overall classification accuracy = 92.19%, Overall kappa statistics = 0.9068.

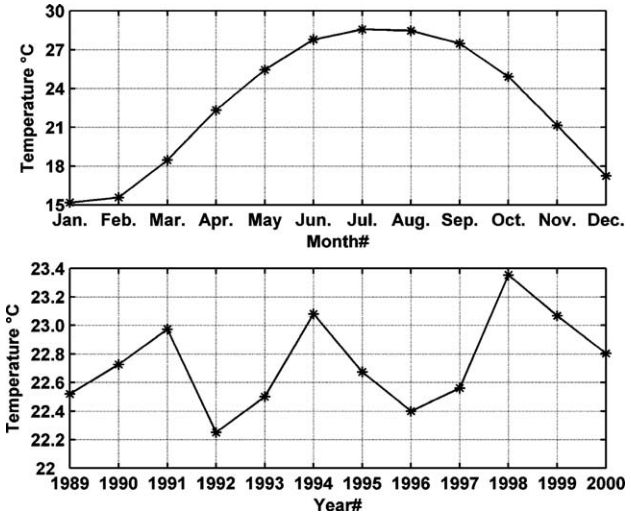

Fig. 4. Fluctuations of yearly and monthly mean temperature from 1989 to 2000, mean value is calculated using the data of weather stations.

area. This study showed that the NDWI was in direct proportion to the water content of vegetation (Fig. 10(a) and (d)).

$$\mathrm{NDWI} = (\rho(band4) - \rho(band5))/(\rho(band4) + \rho(band5)) \tag{7}$$

where, ρ represents the radiance in reflectance units, band3, band4 and band5 represent the spectral bands of the Landsat images.

Another index, NDBI (Zha et al., 2003) in Eq. (8), was introduced in this study, which is sensitive to the built-up area.

$$\mathrm{NDBI} = (d(band5) - d(band4))/(d(band5) + d(band5)) \tag{8}$$

To retrieve bare land from the Landsat imagery, a new index, Normalized Difference Bareness Index (NDBaI) was proposed by this paper's authors as follows (Zhao & Chen, 2005):

$$\mathrm{NDBaI} = (d(band5) - d(band6))/(d(band5) + d(band6)) \tag{9}$$

where, d represents the digital numbers (DNs) of the relevant Landsat TM or ETM+ bands. NDBaI was proposed by analyzing the spectral characteristics of different land use/cover types. Fig. 3 shows that spectral characteristic of band5 − band6 > 0 is highly consistent with bare land. So bare land (Inc. beach, bare land, and land under development) could be distinguished by images with NDBaI > 0, which also refers to primary bare land. At the same time, NDBaI could be used to classify different bare lands (e.g. primary bare land and secondary bare land) according to different values of NDBaI (Table 1).

These indices could be used to classify different land use/cover types (e.g., vegetation, water, built-up) by setting the appropriate threshold values (Table 1 and Fig. 10).

Index value ranges for these land-cover types are not constant, which will have little changes in different regions or in different conditions of atmosphere and precipitation. Sometimes, several

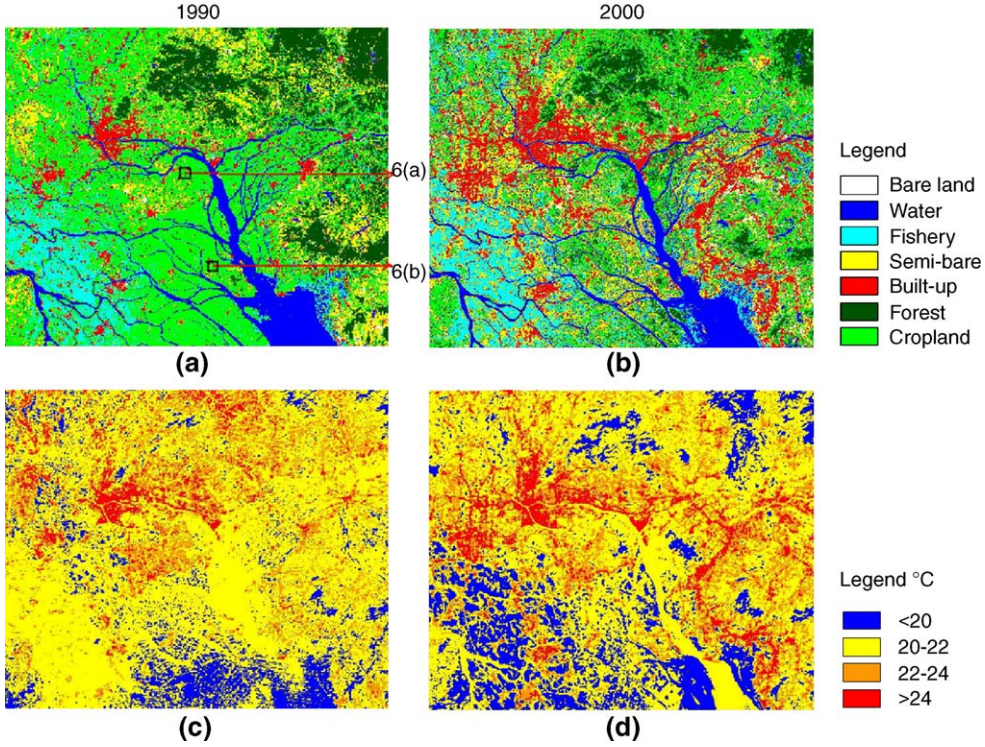

Fig. 5. Land use/cover pattern and temperature distribution in the PRD region on Oct. 13, 1990 and Nov. 1, 2000, (a) land use/cover patterns on Oct. 13, 1990, (b) land use/cover patterns on Nov. 1, 2000, (c) temperature on Oct. 13, 1990, and (d) temperature on Nov. 1, 2000. The boxes in (a) are the locations of the examples for grassland degradation and crop harvest shown in Fig. 6.

Table 3
LUCC in PRD from 1990 to 2000

Land-cover types	Built-up	Water	Fish pond	Semi-bare land	Forest	Cropland	Bare land
1990 (%)	6.09	9.39	10.75	16.33	14.5	42.23	0.72
2000 (%)	13.08	9.52	15.1	28.54	9.6	21.48	2.68
Changes (%)	6.98	0.13	4.35	12.22	−4.9	−20.74	1.97

* Percent data were calculated by dividing the total study area into the pixel area of a given land use/cover type.

indices are integrated to differentiate different land use/cover types.

2.5. Retrieval of land use/cover patterns and the temperature

Indices of NDVI, NDWI, NDBI and NDBaI are used in the classification of images but it was difficult to determine the appropriate threshold values for the indices to get ideal results of classification. In order to solve this problem we analyzed the relative spectral characteristics of different land use/cover types. Here we take the Landsat 7 ETM+ 1G image on Nov. 1, 2000 as an example for the spectral analyses. Through repeated sampling of the representative pixels of each type, the values in all seven bands were obtained and averaged (Fig. 3).

After the spectral characteristics of land use/cover types were identified, Boolean operators were used on the spectral bands to improve the results of indices. For example, an operator (band4 − band5) > 0 was combined with (band4 − band3) > 0 (or NDVI > 0) to extract vegetation from the Landsat imagery because only vegetation has the spectral feature of band4 − band3 > 0 and band4 − band5 > 0. Similarly, water was extracted by combining (band3 − band4) > with (band4 − band5) > 0. We then calculated the intersection of (band3 − band4) > 0, (band4 − band5) > 0, and NDWI > k (k is an estimated value to derive water areas) to retrieve all water bodies in the study area. Then band ratio (band5/band2) was used to divide the total water area into open water surface and fish pond (shallow water areas) by setting the appropriate thresholds. Built-up areas were derived by combining (band4 − band3) < 0 and (band4 − band5) < 0 with NDBI, where determination of an appropriate threshold of NDBI is important. But it is not enough to differentiate the bare land and the built-up area since both have similar spectral characteristics. Then the NDBaI index was used to extract semi-bare land and bare land, which includes land under development and beach. Fig. 3 shows that the spectral disparity is largest in band5 but least in band6 for all selected land use/cover types, and only bare land has the characteristic of band5 − band6 > 0. So the NDBaI index (Eq. (9)) is sensitive to distinguish bare land and semi-bare land.

The mean temperature of every land use/cover type was calculated for analyzing their relationships. At the same time, it was necessary to calculate the mean temperature for specific value ranges of the indices. The relationship between a given index and the corresponding mean temperature was determined by using regression analysis.

3. Results and discussion

3.1. Relationship between urban heat island and land use/cover changes at the regional level

3.1.1. Land use/cover patterns in the PRD region

The threshold approach in combination with the Boolean operators based on band DNs and indices worked very well in identifying land use/cover types. In comparison with traditional image classification methods, such as automated supervised and unsupervised classifications, our method achieved relatively high accuracy. Table 2 represents the error matrix and accuracy assessment for the classification of image on Nov. 1, 2000. The sampling points were randomly taken across the study area, also relatively uniformly distributed among these land use/cover types. The overall accuracy of classification is approximately 92%. Among selected 7 land use/cover types, the classification performed best for bare land, water, and fish pond, but less so for forest and built-up area.

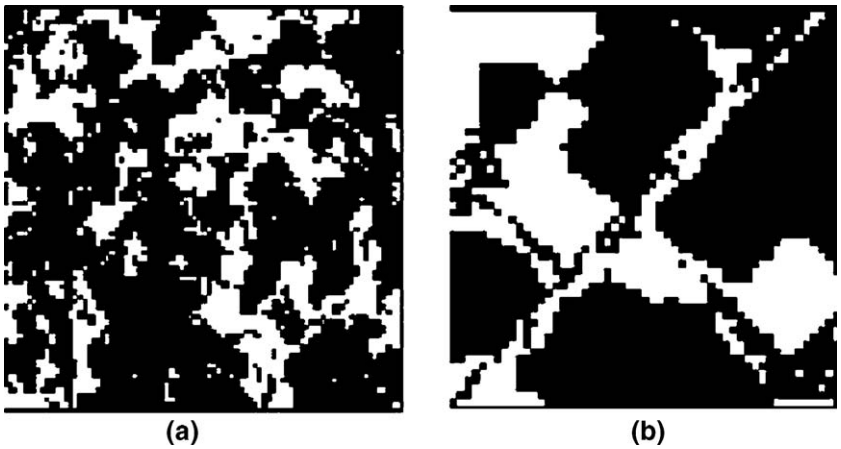

Fig. 6. Changes of grassland degradation (a) and seasonal bare cropland (b) from 1990 to 2000. The white color represents the bare land in 2000 converted from other land use/cover types in 1990. (a) The bare land in 2000 was caused by degradation of grassland located in Panyu. (b) The bare land in 2000 was caused by crop-harvesting. Both sample areas are shown in Fig. 5(a).

Table 4
Temperature difference between different land use/cover types in PRD (°C)

Date	Types					
	$B-V^{(1)}$	$B-W^{(2)}$	$B-D^{(3)}$	$B-F^{(4)}$	$B-C^{(5)}$	$B-A^{(6)}$
Oct. 13, 1990	2.55	2.884	−0.02	2.49	2.65	2.32
Oct. 29, 1994	0.45	2.06	0.09	1.758	0.01	0.46
Mar. 3, 1996	0.65	3.47	−0.06	1.47	0.54	0.66
Sept. 14, 2000	3.089	3.973	1.094	3.471	2.29	2.59
Nov. 1, 2000	3.33	3.46	1.62	3.7	2.63	2.76

(1) $B-V$ represents the temperature difference between built-up area and vegetation. (2) $B-W$ represents the difference between built-up area and water. (3) $B-D$ represents the difference between built-up area and development. (4) $B-V$ represents the difference between built-up area and fish pond. (5) $B-C$ represents the difference between built-up area and cropland. (6) $B-A$ represents the difference of built-up area and suburban areas.

Table 5
Rainfall before acquisition times of images

Station	Yangjiang	Wuzhou	Guangzhou	Heyuan	Shanwei	Hong Kong
1990/9/4–10/13 (mm)	256.2	103.4	115.8	222.1	349.2	501.3
1994/9/20–10/29 (mm)	124.2	237.4	18.7	38.5	164.4	92.0
1996/1/24–3/3 (mm)	92.5	52.1	46.6	63.4	22.3	27.4
2000/8/15–9/14 (mm)	128.6	45.3	105.1	259.2	307.7	446.8
2000/9/23–11/1 (mm)	242.4	64.8	304.8	109	54.7	204.1

3.1.2. Temperature variation over different land use/cover types in the pRD region

We used temperature data from weather stations shown in Fig. 1 to examine the seasonal and inter-annual variation in temperature during the study period. There were significant inter-annual and monthly/seasonal fluctuations of temperature in the PRD region from 1990 to 2000 (Fig. 4). It is shown in Fig. 4 that the annual mean temperature had an increase trend in the process of fluctuations for the past 10 years. To study the effect of human activities on global warming, it is necessary to study the changes of temperature with LUCC.

In this study, we selected five Landsat images, i.e., the Landsat 5 TM images on Oct. 13, 1990, Oct. 29, 1994 and Mar. 3, 1996, respectively, and Landsat 7 ETM+ images on Sept. 14, 2000 and Nov. 1, 2000, respectively. The distribution pattern of urbanized areas has been changed from a dot pattern in 1990 to a chain/areal pattern in 2000, with a result of gradually formed and increased infrastructure of the current urban system in the PRD region during the study period. A comparison between land use/cover maps derived from images of Oct. 13, 1990 and Nov. 1, 2000 revealed dramatic expansion of the urbanized area (Fig. 5).

It was found that the UHI intensity changed with the shifts of seasons, and agricultural activities had an obvious influence on the interpretation of land use/cover types. In order to minimize the impact of seasonal difference, two images on Oct. 13, 1990 and Nov. 1, 2000 were selected to study the relationships between LUCC and UHI and compare the UHI intensity in the PRD region for the past 10 years. Land use/cover types and temperature were retrieved from Landsat images to analyze the changes of temperature distributions for the past 10 years. To study the temperature relationships of different land use/cover types, the mean temperatures of different land use/cover patterns

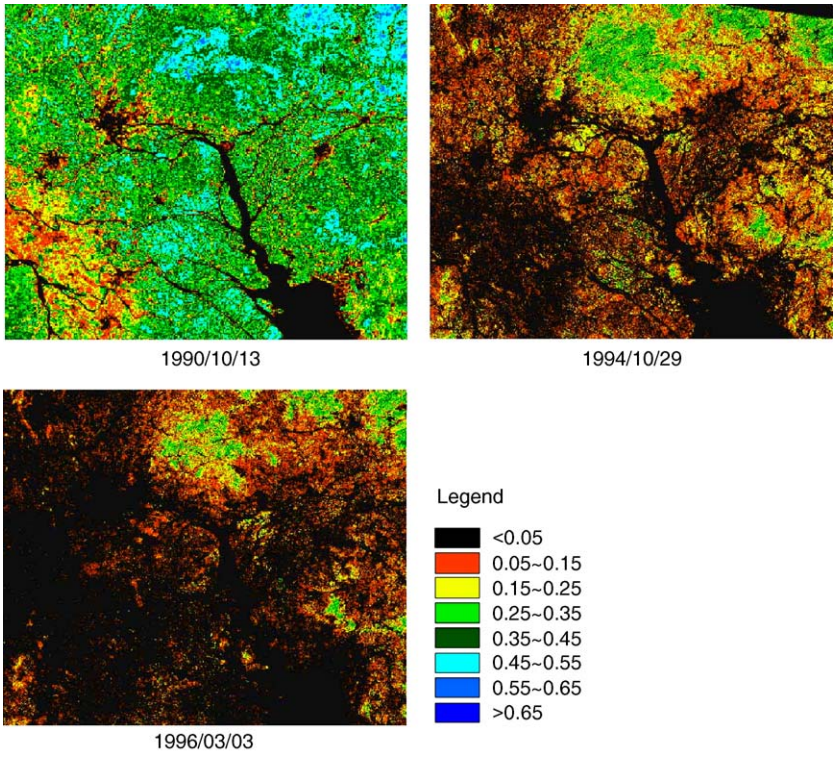

Fig. 7. NDVI distributions in the PRD region on Oct. 13, 1990, Oct. 29, 1994 and Mar. 3, 1996, respectively.

Table 6
Contribution of temperature for each land use/cover types to the regional temperature (PRD)

Land use/cover	dT	Scenario 1 (past)	Contribution	Scenario 2 (1990)	Contribution	Scenario 3(2000)	Contribution	Scenario 4 (2010)	Contribution
Built-up	1.56	0	0	6.1	0.095	13.1	0.204	28.1	0.438
Water	−1.58	9.48	−0.150	9.4	−0.149	9.5	−0.150	7.9	−0.125
Fish pond	−0.99	14.3	−0.142	10.8	−0.107	15.1	−0.149	12.49	−0.124
Semi-bare land	0.79	0	0	16.3	0.129	28.5	0.225	23.57	0.186
Forest	−0.42	19.29	−0.081	14.5	−0.061	9.6	−0.040	7.9	−0.033
Cropland	−0.34	56.18	−0.191	42.2	−0.143	21.5	−0.073	17.8	−0.061
Bare land	0.98	0.75	0.007	0.7	0.007	2.7	0.027	2.24	0.022
Total		100	22.443	100	22.771	100	23.043	100	23.303

Note, dT has a unit of °C, scenario represents the percentage of every land use/cover type for different time periods (past, current and future), and contribution is a multiplication of dT and scenario, as well as in Table 7.

were derived by averaging all corresponding pixel values. Fig. 5 showed the results derived from Landsat images on Oct. 13, 1990 and Nov. 1, 2000, respectively.

The results in Fig. 5(c) and (d) suggest that the spatial pattern of the heat islands (areas with relatively high temperatures) has changed from a scattered pattern (bare land, semi-bare land and urban area were warmer than other areas) in 1990 to a more contiguous pattern of urban heat islands in 2000, along with the expansion of the regional urban system. The centers of high temperature were consistent with built-up areas, which can be seen by comparing land use/cover with temperature maps (Fig. 5, (a) vs. (c), and (b) vs. (d)).

An analysis based on the interpretation of land use/cover types showed two obvious changes, percentage-wise, between the two image dates. The percent of built-up area increased from 6.09% in 1990 to 13.08% in 2000, more than doubling the size of the urbanized areas, while the percent of cropland decreased from 42.23% to 21.48% for the same time span (Table 3). Much of the cropland in the region was unplanted or ill-managed, and at the same time, forest and grassland were degraded seriously (Fig. 6(a)) in the process of urbanization.

Bare and semi-bare lands caused by vegetation degradation often have a scattered pattern and irregular shapes, as the white patches seen in Fig. 6(a). Agricultural activities in the region can also play an important role in image interpretation. The date of Oct. 13, 1990 fell in the late part of crop growing season, while Nov. 1, 2000 was during the harvest time when the water content of vegetation was low and some of the crops were already harvested. Fig. 6(b) is a representative sample, where the cropland in 1990 was classified as bare land in 2000 because of crop harvest. The combination of urban development, crop rotation, ill-managed cropland, and vegetation degradation may have caused increases in bare land and semi-bare land, especially the latter, which can also be seen from Table 3.

Land use/cover changes have caused changes in the temperature field in the PRD region. Mean temperature of

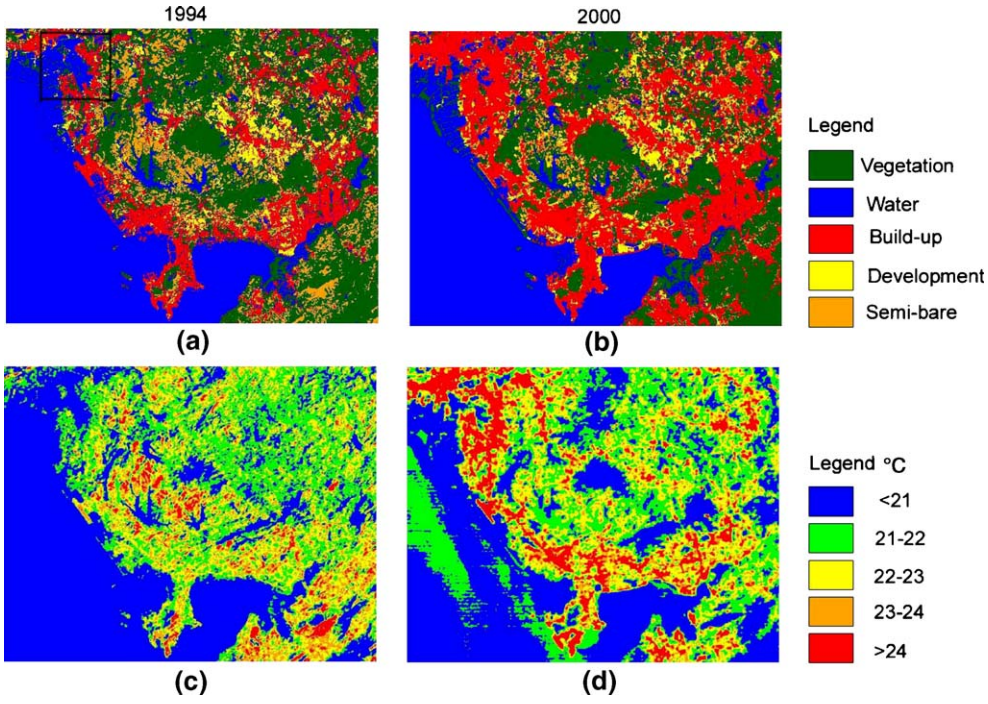

Fig. 8. Land use/cover patterns and temperature in Shenzhen retrieved from Oct. 29, 1994 and ETM+ image on Nov. 1, 2000, respectively. *(a) and (b) are land use/cover patterns on Oct. 29, 1994 and Nov.1, 2000, respectively; (c) and (d) are temperatures derived from the 1994 and 2000 images. Black frame in (a) is a sample showing a change from waters in 1990 to built-up area in 2000.

Table 7
Contribution of temperature for each land use/cover types to the local temperature (Shenzhen)

Land use/cover	dT	Scenario 1 (past)	Contrib.	Scenario 2 (1994)	Contrib.	Scenario 3 (1996)	Contrib.	Scenario 4 (1998)	Contrib.	Scenario 5 (2000)	Contrib.	Scenario 6 (2006)	Contrib.
Vegetation	−0.54	58	−0.313	41.76	−0.226	39.24	−0.212	41.22	−0.223	37.15	−0.201	28.49	−0.154
Water	−2.09	21	−0.439	20.35	−0.425	16.76	−0.350	13.73	−0.287	14.18	−0.296	10.88	−0.227
Built-up	0.76	0	0	20.55	0.156	23.26	0.177	26.34	0.200	35.58	0.270	50.61	0.385
Development	0.23	0	0	6.96	0.016	9.65	0.022	9.09	0.021	4.66	0.011	3.57	0.008
Semi-bare	0.7	21	0.147	10.38	0.073	11.09	0.078	9.62	0.067	8.43	0.059	6.45	0.045
Total		100	22.395	100	22.594	100	22.715	100	22.778	100	22.843	100	23.057

every land use/cover type was calculated by averaging all corresponding pixel of a given land use/cover type. Considering the difference in temperature and atmospheric conditions between acquisition times of the Landsat images, we used the UHI intensity in our analysis, rather than looking at the absolute land surface temperature changes. Since the study region has a significant portion as open water surface (Table 3) and temperature variation over water tends to be less variable due to its high heat capacity, we can use the difference in temperature between urban area and waters as the measure of the UHI intensity. In this paper, the difference in temperature between different land use/cover types were also used as references (Table 4). To help in the interpretation of the results, we also calculated the mean UHI intensity for each image (Table 4).

Although there was a general trend of increasing intensity of UHI in the PRD region, apparently the UHI intensity in 1990 is greater than that in 1994 and 1996 even though the urban area had increased consistently since the early 1990s. Such disparity could be explained by the changes in suburban vegetation/crop condition and its water content. Our analysis indicated that vegetation density and its coverage on Oct. 13, 1990 were greater than that on Oct. 29, 1994 and Mar. 3, 1996, which could be the result of seasonal variations or agricultural activities because one image on Mar. 3, 1996 was in the early spring time before young crops reached full coverage of the ground, while the other one on Oct. 13, 1990 was late in the growing season and close to harvest. Fig. 7 shows the NDVI distributions on Oct. 13, 1990, Oct. 29, 1994 and Mar. 3, 1996, from which we can also see that the vegetation density on Oct. 13, 1990 was greater than that on Oct. 29, 1994 and Mar. 3, 1996. At the same time, soil moisture and VWC on the 1990 image date were higher than that on the 1996 and 1994 image dates, which is evident from a 40-day rainfall amount prior to the image acquisition time (Table 5). From our analysis, it can be seen that the UHI intensity in the study region was influenced by multiple factors. From the decreased UHI, we can conclude that UHI intensity was related with the density of vegetation, moisture of study area and vegetation cover areas except for urban size (Section 3.3).

From the above analysis, it can be seen that UHI intensity can be influenced by many factors and it may not always present a linear trend with the expansion of urban area. Table 4 shows the temporal trend of relative UHI intensity determined by the mean temperature difference between built-up area and the other land use/cover types except for semi-bare land. The relative UHI intensity is obviously intensified by more than 0.8 °C (considering great difference of the above mentioned impact factors, statistical data of images on Oct. 29, 1994 and Mar. 3, 1996 were not taken into consideration). Temperature difference between urban and suburban area ($B-A$s in Table 4) showed that the intensity of UHI increased only 0.44 °C, then it could be concluded that the increase of semi-bare land would weaken the UHI effect, but make great contributions to the regional temperature (Table 6). We also calculated the mean temperature differences of the land use/cover types to the mean regional temperature. Using this information, we can estimate how changes in land use/cover pattern may have contributed to the regional temperature. Assuming a regional mean temperature as the long-term mean temperature of the spring and fall seasons in the study region (23 °C), and an initial land use/cover pattern with no urban built-up area and dominated by forest and cropland, we can estimate the contribution of temperature for each land use/cover type to the regional temperature (Table 6) and obtain a new regional temperature adjusted by the land use/cover pattern. Similarly, we calculated the adjusted regional temperature based on the 1990, 2000, and a future land use/cover pattern. Table 6 lists the regional mean temperature adjusted to changes in land use/cover patterns for the PRD region under several scenarios. For the past scenario, urban built-up area and semi-bare land caused by urbanization were assumed to zero and assigned them to other land use/cover types by scale in 1990. For a future 10-year scenario, we assumed that urban built-up areas would be increased by the same proportion as the past 10 years from 1990 to 2000, the increased built-up area come from the other land use/cover types by scale in 2000. The column dT is the mean temperature difference of a given land use/cover type to mean temperature across the entire study region of all image dates. It is concluded that land use/cover changes can bring significant temperature increases, which are

Table 8
Temperature difference between different land use/cover types in Shenzhen

Types	$B-V^{(1)}$	$B-W^{(2)}$	$B-D^{(3)}$	$B-S^{(4)}$	$B-A^{(5)}$
Oct. 29, 1994	0.24	2.07	0.31	−1.32	0.46
Mar. 3, 1996	0.34	2.58	0.24	−0.44	0.60
Dec. 22, 1998	0.31	2.24	0.06	−0.38	0.54
Nov. 1, 2000	1.98	2.72	1.02	0.63	1.89

(1) $B-V$ represents the temperature difference between built-up area and vegetation. (2) $B-W$ represents the difference between built-up area and water, which only include inshore water and inland water. (3) $B-D$ represents the difference between built-up area and development. (4) $B-S$ represents the difference between built-up area and semi-bare land.

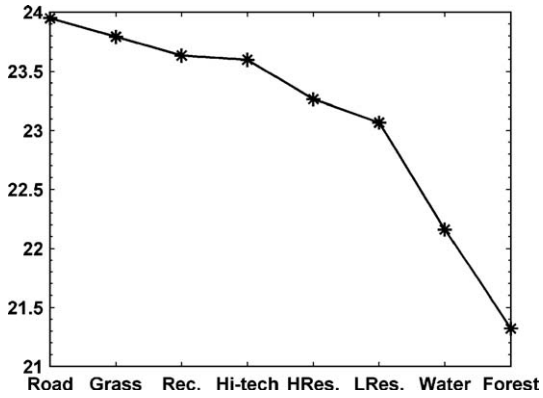

Fig. 9. Mean temperature of different land use/cover types in downtown area derived from Landsat ETM+ thermal band on Nov. 1, 2000. Rec.=Recreational area; HRes.=High density residential areas; LRes=Low density residential areas.

conformed by the changes of the total contributions of land use/cover in Table 6.

It could be found from Table 6 that the contribution of temperature for the types of built-up and water was higher, followed by fish pond and bare land in the Pearl River Delta. As the water changed less during the study time period, it had less influence on regional temperature changes. Expansions of built-up area became the main contributor for the regional temperature rise (0.11 °C). Although the semi-bare land was not big for its contribution of temperature per unit area, it still became an important contributor to the temperature rise (0.10 °C) because of its large area change. The calculated results showed that the contribution of semi-bare land was almost equal to that of built-up type, both of them contributed more than 75% (0.21 °C) to the regional temperature rise (0.27 °C) in the Pearl River Delta. If the contribution of cropland (0.07 °C) was included, it nearly matched the regional total contribution. The results suggested that the impact of land use/cover change on temperature rise mainly occurred in the types of built-up, semi-bare land and cropland, where great area changes had happened over the study time period in the Pearl River Delta. As the changes of semi-bare land and cropland were largely caused by urbanization, it could be concluded that urbanization was a major contributor to the regional temperature rise. If the future 10 years' urban area expands in same rate as that in the time period of 1990 to 2000, the contribution of land use/cover changes to the regional temperature rise will reach almost 1 °C when urban area expanded from 0 to 30 percent in the PRD (Table 6).

3.2. Relationship between urban heat island and land use/cover changes at local level

3.2.1. Temperature variations for different land use/cover patterns in Shenzhen

In this paper, Shenzhen, including urban and suburban areas experienced the fastest urbanization since 1980s, as well as land use/cover changes, was taken as a case to explore the effect of UHI for different land use/cover types in a big city. It was reported that the intensity of UHI in Shenzhen had a seasonal variation pattern, with higher average temperatures in autumn and winter than that in spring and summer (Kim & Baik, 2002; Zhong, 1996). Following this situation, Landsat TM image on Oct. 29, 1994 and ETM+ image on Nov. 1, 2000 were selected to examine the variation of average temperature and the detailed distribution of UHI, considering a rapid urbanization during that

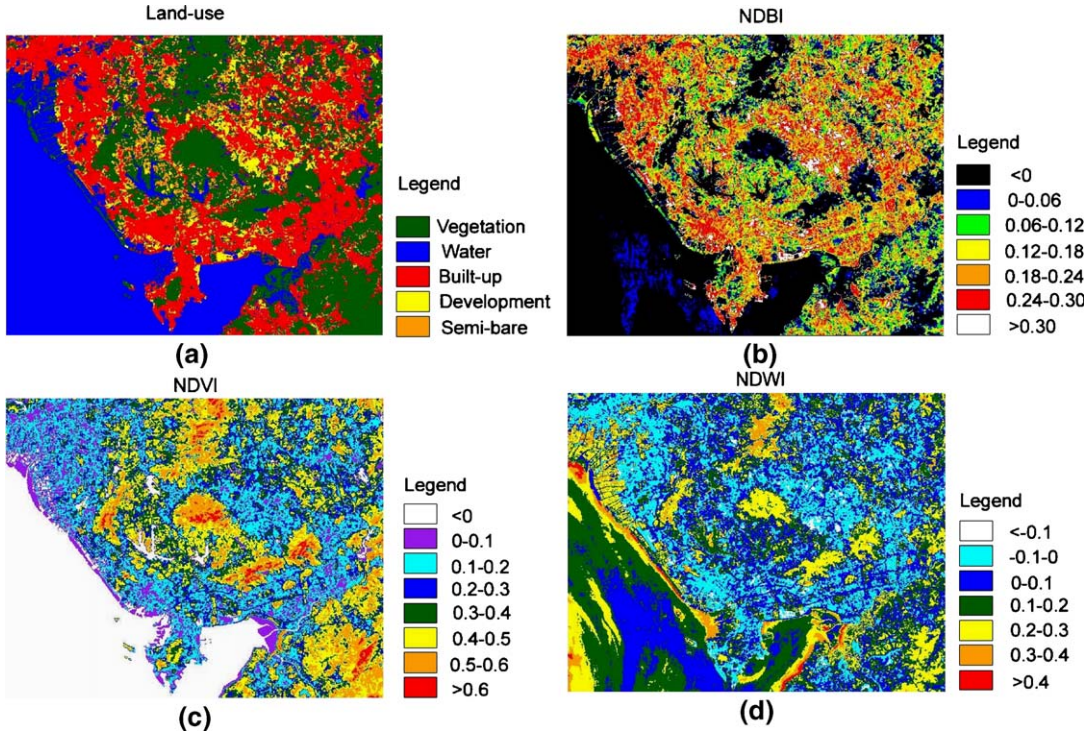

Fig. 10. Maps of land use/cover types (a), NDBI (b), NDVI (c), and NDWI (d) indices in Shenzhen derived from Landsat ETM+ image on Nov. 1, 2000.

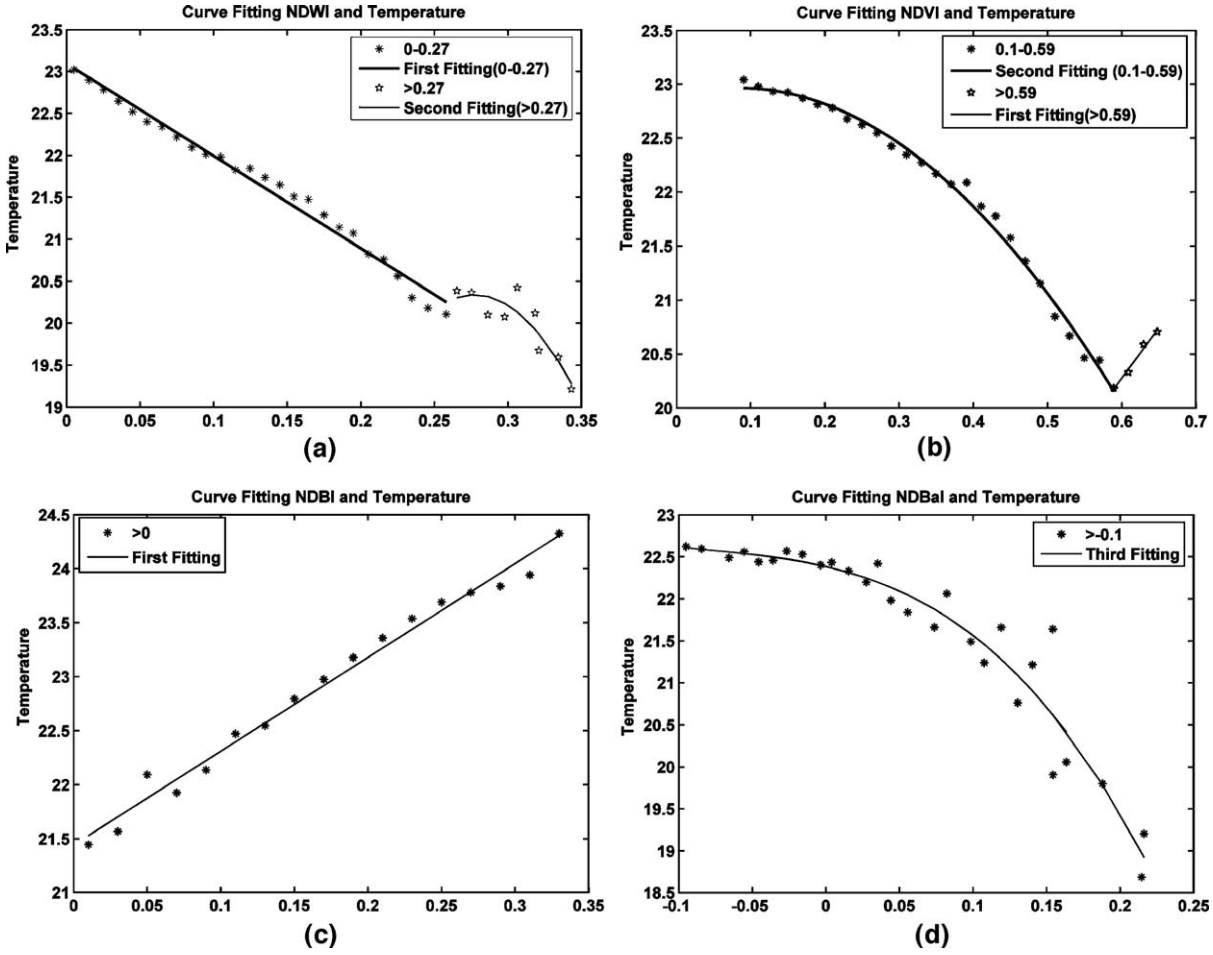

Fig. 11. Relationships between temperature and index values, averaged by index values of 0.01 intervals for Shenzhen. (a) NDWI and temperature, (b) NDVI and temperature, (c) NDBI and temperature, (d) NDBaI and temperature.

time period. The analysis of the relationship between land use/cover types and temperature in the PRD showed that the temperature difference between forest and cropland (e.g. 1990) was so small that could be neglected when the cropland was covered by growing and exuberant crop, as well as the water area and fish pond. So only five land use/cover types were classified in Shenzhen (i.e. vegetation, water, built-up, development area and semi-bare land). Vegetation is the area by forest, shrub and crop. Water includes fish ponds (shallow water areas) and water bodies in the city area. Area under development is similar to bare land in the PRD. Maps of land use/cover (Fig. 8(a) and (b)) and temperature (Fig. 8(c) and (d)) were retrieved from Landsat TM and ETM+ images Oct. 29, 1994 and Nov. 1, 2000, respectively, using the same methods as described earlier.

The trend of UHI in Shenzhen had a similar variation pattern to that of the Pearl River Delta region, but showed a more obvious trend: when the urban area expanded, built-up area increased obviously while other land use/cover types had a consistent decrease (Table 7), which indicates the autumn of urbanization in Shenzhen. The temperature differences between different land use/cover types were retrieved from Landsat TM images on Oct. 29, 1994, Mar. 3, 1996 and Dec. 22, 1998, and Landsat ETM+ images on Nov. 1, 2000, respectively, to study the changes of UHI intensity (Table 8). Comparison between values of $B-A$ in Tables 4 and 8 showed that UHI intensity of the PRD on Oct. 29, 1994 and Mar. 3, 1996 were approximately same to that of Shenzhen, but the UHI intensity in the PRD was greater than that in Shenzhen on Nov. 1, 2000. Contributions of land use/cover change in Shenzhen were listed in Table 7. It is shown that land use/cover changes, especially urban expansion and reclaiming land from sea have made greater contributions to temperature rise in Shenzhen. The black box in Fig. 8(a) is a sample area, where water area in 1994 was greatly changed into built-up area in 2000 (Table 6). The total annual contribution of land use/cover changes in Shenzhen (0.042 °C) was obviously greater than that in the PRD (0.027 °C). It suggested that the rapid urbanization would make greater contribution to global warming. From the above analysis, it could be concluded that land use/cover change would influence the global warming and UHI distributions. But proper land use planning could weaken temperature rise, for example, positive contributive land use/cover types (e.g., semi-bare land and area under development) were occupied when the urban area was expanded.

3.2.2. Temperature variations for different land use/cover patterns in the Special Economic Zone (SEZ) of Shenzhen

Fig. 9(d) showed that higher temperature did not distribute over all the built-up area in Shenzhen, and it was really fragmentized. It

Table 9
Regression parameters in different value ranges

	NDWI − T*		NDVI − T*		NDBI − T*	NDBaI − T*
	0<NDWI<0.27	NDWI>0.27	0.1<NDVI<0.59	NDVI>0.59	NDBI>0	NDBaI>−0.1
*r	−0.9921	−0.8355	−0.9645	0.9914	0.9928	−0.8891
R^2	0.9842	0.8195	0.9936	0.9830	0.9848	0.9259

*r = correlation coefficient, T = temperature, NDWI − T, NDVI − T, NDBI − T and NDBaI − T refer to the regression between NDWI, NDVI, NDBI, NDBaI and temperature respectively.

is necessary to study the distribution patterns of heat island within the urbanized areas. In this section, Luohu, Futian and Nanshan Districts of Shenzhen SEZ were taken as examples to study temperature changes in a city. Luohu is in the eastern part of the Special Economic Zone. It is Shenzhen's financial and trade center and the base for network services, where the building and population densities are higher than those in the other districts. Futian is the center of administration, culture, information, exhibition and commerce. Nanshan District is the center of hi-tech industry, higher education, and logistics in Shenzhen.

The urban area was classified into eight land use/cover types: road, vegetation (forest and grassland), water, residential area in low and high density, recreational area, and industrial area (High-tech area). Mean temperature of different land use types is calculated by sampling the representative pixels of each of these land use/cover types on the Landsat image of Nov. 1, 2000. Results were shown in Fig. 9. In the process of classification and calculation, digital line graphs (DLG) at the scale of 1:10,000 and the IKONOS image were used to identify different land-cover types.

The results in Fig. 9 showed that the highest temperature in the city was found in the area of road, followed by grassland or brushes, which was mainly distributed within the residential area, recreational area (e.g., golf course) or along the roads and streets. The recreational area (e.g., artificial pleasure ground and playground) became the third highest temperature area because of lots of impervious surfaces and frequent human activities. The temperature of the hi-tech industrial area, which often contains much bare land and impervious surface, is also higher than that of the high density residential area. Water and forest area, mostly located in parks, had the lowest temperatures. The detailed analysis of land use types within the urban areas indicate that high densities of impervious surface, population density and frequent human activities contribute to the UHI intensity. Therefore, it is possible to alleviate urban heat island effect by optimizing land use planning.

3.3. Relationship between temperature and indices, NDWI, NDVI, NDBI and NDBaI

Fig. 10 shows the maps of the NDWI, NDVI, NDBI indices in comparison with the land use/cover map retrieved from Landsat ETM+ image on Nov. 1, 2000, from which we can see the corresponding relationships between indices and land use/cover types. Previous analyses have clearly indicated the relationship between land use/cover types and the temperature spatial variation pattern in the study region. Previous studies have suggested that NDVI is strongly correlated to surface temperature retrieved from Landsat images. Since in our study, we used NDWI, NDVI, NDBI, and NDBaI in land use/cover classification, we would like to see if there are quantifiable relationships between temperature and these indices. We queried out pixels of index values by 0.01 intervals and then averaged the corresponding pixels for their temperature values. The results are presented in Fig. 11.

Previous studies of relationship between vegetation and temperature (e.g. Carlson et al., 1994, 1995; Owen et al., 1998; Sandholt, Rasmussen, & Andersen, 2002) have proposed a new method: 'triangle method', by which the relationships of three parameters, (i.e., vegetation, surface moisture availability and temperature) were discussed. In that study, scatter plots were used to study the relationships between NDVI and temperature, but not present the relationships quantitatively. In this section, NDWI was used to substitute for the surface moisture availability, NDVI for the vegetation, then negative correlations were found between NDWI, NDVI and temperature when NDVI is limited in less than 0.6. But when NDVI reaches 0.6 or more, where 100 percent vegetation cover was identified, a linear positive correlation between NDVI and temperature was found Compared with the 'triangle method', the regression analysis between NDWI, NDVI and temperature present the relationships quantitatively and clearly (Eqs. (10) and (11)).

$$\begin{aligned} T &= -11.0034\mathrm{NDWI} + 23.0926 \quad (\mathrm{NDWI} \in (0, 0.27)) \\ T &= -243.2049\mathrm{NDWI}^2 + 134.8284\mathrm{NDWI} \\ &\quad +1.6539 \quad (\mathrm{NDWI} \geq 0.27) \end{aligned} \tag{10}$$

$$\begin{aligned} T &= -11.0039\mathrm{NDVI}^2 + 1.8511\mathrm{NDVI} \\ &\quad +22.8865 \quad (\mathrm{NDVI} \in (0.1, 0.59)) \\ T &= 9.2727\mathrm{NDVI} + 14.7147 \quad (\mathrm{NDVI} > 0.59) \end{aligned} \tag{11}$$

Dousset and Gourmelon (2003) studied the relationships between urban surface temperature and land use/cover types by analyzing satellite multi-sensor data, who presented the correlations between densely built class and nighttime/daytime average LST with scatter plot, in which some exceptional pixels (e.g., cloud contaminated pixels) will be introduced, which influenced the correlation analysis. In order to analyze the correlation between the density of built-up area and its temperature accurately, NDBI was used and averaged values of NDBI and corresponding temperature by intervals of 0.01, by

which the influence of exceptional pixels will be removed. Their relationship indicated a statistically significance (Table 9) and the regression equation was listed as follows:

$$T = 8.6854\mathrm{NDBI} + 21.4420 \quad (12)$$

Price (1990) found that predominantly bare soil locations experienced a wider variation in surface radiant temperature than densely vegetated locations. But there were no further efforts to study the impact of bare soil on the temperature. In this paper, we studied it quantitatively by using the proposed NDBaI. Unexpectedly, great negative correlation and wider variations of temperature were found in the analysis, which might be contributed by the physical characteristics of soil in the bare land. Its regression equation was given as follows.

$$T = 119.7003\mathrm{NDBaI}^3 - 29.3593\mathrm{NDBaI}^2 - 4.0608\mathrm{NDBaI} + 22.3848 \quad (\mathrm{NDBaI} > -0.1) \quad (13)$$

Where, T refers to the mean temperature, as well as Ts in Eqs. (10)–(12). The regression parameters were shown in Table 9 and significant correlations between indices and temperature were found.

4. Conclusions

In this paper, qualitative and quantitative analyses have been used to study the relationship between LUCC and UHI. The analyses were focused on regional (in the PRD) and local (in Shenzhen and the SEZ of Shenzhen) levels, respectively, and several conclusions were made: (1) distribution of heat island has been changed from mixed pattern to UHI as the urbanized area expanded rapidly in PRD and Shenzhen; (2) LUCC contributed to the global warming and affected UHI intensity mainly through the processes of urban sprawl, degradation of cropland and sea reclamation in the study area; (3) UHI intensity changes with the air temperature that was proven by the higher UHI intensity on Sept. 14, 2000 compared with that on Nov. 1, 2000 in both regional and local levels in this study. Humidity would be another important impact factor to UHI intensity, and the UHI would be weaker when the study area is arid; (4) UHI was proportionally related with urban size, population density and frequent activities according to the analysis in the local level; and (5) quantitative analysis between temperature and indices showed that great differences of temperature even existed in a land use/cover type except for variations between different land use/cover types.

All the analyses in this paper were based on the interpretation of remote sensing images, by which we analyzed not only the phenomenon of UHI but the impact factors of UHI from the regional level to the local level. The temporal and spatial variations of UHI have been concluded by the analysis of multi-temporal remote sensing images. The results showed that although remote sensing images were ideal for analyzing UHI, it is difficult to select images with similar conditions of atmosphere, hydrology and vegetation cover areas. If the analysis is based on regional level, uniform atmosphere condition is necessary for the retrieval of temperature, which would be more difficult to select proper images.

In future study, several works need to be further focused. Firstly, the retrieval method of temperature needs to be improved to reduce the influence of thin cloud and inhomogeneous atmosphere condition. Secondly, the impact of the distribution pattern of different land use/cover types in the urbanized area on UHI needs to be further studied. Thirdly, the difference of urban size between inland and coastal areas in different climate conditions would be compared its formation of UHI. Fourthly, it should be important to investigate the effect of human activities and other impact factors on decreasing the contributions of UHI to global warming and finally, the errors caused by different conditions in every land use/cover type need to be more accurately estimated or removed.

Acknowledgement

This work was funded by the 973 Program (Grant No. 2003CB415205), the National Natural Science Foundation of China (Grant No. 40176032), the Opening Foundation of LED, South China Sea Institute of Oceanography, Chinese Academy of Sciences and the open fund by the Key Lab of Poyang Lake Ecological Environment and Resource Development, Jiangxi Normal University in China (Grant No. 200401006(1)).

References

Carlson, T. N., Gillies, R. R., & Perry, E. M. (1994). A method to make use of thermal infrared temperature and NDVI measurements to infer surface soil water content and fractional vegetation cover. *Remote Sensing Reviews*, *9*, 161–173.

Carlson, T. N., Gillies, R. R., & Schmugge, T. (1995). An interpretation of methodologies for indirect measurement of soil water content. *Agricultural and Forest Meteorology*, *77*, 191–205.

Ceccato, P., Flasse, S., & Gregoire, J. (2002). Designing a spectral index to estimate vegetation water content from remote sensing data: Part 2. Validation and applications. *Remote Sensing of Environment*, *82*, 198–207.

Chen, Z. M., Babiker, I. S., Chen, Z. X, Komaki, K., Mohamed, M. A. A., & Kato, K. (2004). Estimation of interannual variation in productivity of global vegetation using NDVI data. *International Journal of Remote Sensing*, *25* (16), 3139–3150.

Chen, Yunhao, Wang, Jie, & Li, Xiaobin (2002). A study on urban thermal field in summer based on satellite remote sensing. *Remote Sensing for Land and Resources*, *4*, 55–59.

Dash, P., Gottsche, F. -M., Olesen, F. -S., & Fischer, H. (2002). Land surface temperature and emissivity estimation from passive sensor data: Theory and practice—current trends. *International Journal of Remote Sensing*, *23*(13), 2563–2594.

Deosthali, V. (2000). Impact of rapid urban growth on heat and moisture islands in Pune City, India. *Atmospheric Environment*, *34*, 2745–2754.

Dousset, B., & Gourmelon, F. (2003). Satellite multi-sensor data analysis of urban surface temperatures and landcover. *Photogrammetry and Remote Sensing*, *58*, 43–54.

Gallo, K. P., & Owen, T. W. (1998a). Assessment of urban heat island: A multi-sensor perspective for the Dallas-Ft. Worth, USA region. *Geocarto International*, *13*, 35–41.

Gallo, K. P., & Owen, T. W. (1998b). Satellite-based adjustments for the urban heat island temperature bias. *Journal of Applied Meteorology*, *38*, 806–813.

Gallo, K. P., Tarpley, J. D., McNab, A. L., & Karl, T. R. (1995). Assessment of urban heat islands: A satellite perspective. *Atmospheric Research*, *37*, 37–43.

Gao, Bo-Cai (1996). NDWI — a normalized difference water index for remote sensing of vegetation liquid water from space. *Remote Sensing of Environment*, *58*(3), 257–266.

Giridharan, R., Ganesan, S., & Lau, S. S. Y. (2004). Daytime urban heat island effect in high-rise and high-density residential developments in Hong Kong. *Energy and Buildings*, *36*(6), 525−534.

Hawkins, T. W., Brazel, A. J., Stefanov, W. L., Bigler, W., & Saffell, E. M. (2004). The role of rural variability in urban heat island determination for Phoenix, Arizona. *Journal of Applied Meteorology*, *43*, 476−486.

Jackson, T. J., Chen, D., Cosh, M., Li, F., Anderson, M., Walthall, C., et al. (2004). Vegetation water content mapping using Landsat data derived normalized difference water index for corn and soybeans. *Remote Sensing of Environment*, *92*, 475−482.

Kim, Y. H., & Baik, J. J. (2002). Maximum Urban Heat Island Intensity in Seoul. *Journal of Applied Meteorology*, *41*, 651−653.

Maki, M., Ishiahra, M., & Tamura, M. (2004). Estimation of leaf water status to monitor the risk of forest fires by using remotely sensed data. *Remote Sensing of Environment*, *90*, 441−450.

Nieuwolt, S. (1966). The urban microclimate of Singapore. *The Journal of Tropical Geography*, *22*, 30−37.

Oke, T. R. (1987). *Boundary layer climates* (2nd ed.). London: Methuen (435 pp).

Owen, T. W., Carlson, T. N., & Gillies, R. R. (1998). An assessment of satellite remotely-sensed land cover parameters in quantitatively describing the climatic effect of urbanization. *International Journal of Remote Sensing*, *19*, 1663−1681.

Price, J. C. (1990). Using spatial context in satellite data to infer regional scale evapotranspiration. *I.E.E.E. Transactions on Geoscience and Remote Sensing*, *28*, 940−948.

Purevdorj, T. S., Tateishi, R., Ishiyama, T., & Honda, Y. (1998). Relationships between percent vegetation cover and vegetation indices. *International Journal of Remote Sensing*, *19*(18), 3519−3535.

Rao, P. K. (1972). Remote sensing of urban "heat islands" from an environmental satellite. *Bulletin of the American Meteorological Society*, *53*, 647−648.

Saaroni, Hadas, Eyal, Ben-Dor, Arieh, Bitan, & Oded, Potchter (2000). Spatial distribution and microscale characteristics of the urban heat island in Tel-Aviv. *Landscape and Urban Planning*, *48*, 1−18.

Sandholt, I., Rasmussen, K., & Andersen, J. (2002). A simple interpretation of the surface temperature / vegetation index space for assessment of surface moisture status. *Remote Sensing of Environment*, *79*, 213−224.

Streutker, D. R. (2002). A remote sensing study of the urban heat island of Houston, Texas. *International Journal of Remote Sensing*, *23*(13), 2595−2608.

Streutker, D. R. (2003). Satellite-measured growth of the urban heat island of Houston, Texas. *Remote Sensing of Environment*, *85*, 282−289.

Tian, Qingjiu, & Xiangjun, Min (1998). Advances in study on vegetation indices. *Advance in Earth Sciences*, *13*(4), 327−333.

Wang, J., Rich, P. M., Price, K. P., & Kettle, W. D. (2004). Relations between NDVI and tree productivity in the central Great Plains. *International Journal of Remote Sensing*, *25*(16), 3127−3138.

Weng, Q. (2001). A remote sensing-GIS evaluation of urban expansion and its impact on surface temperature in Zhujiang Delta, China. *International Journal of Remote Sensing*, *22*(10), 1999−2014.

Weng, Q., Lu, Dengsheng, & Jacquelyn, Schubring (2003). Estimation of land surface temperature–vegetation abundance relationship for urban heat island studies. *Remote Sensing of Environment*, *89*, 467−483.

Zarco-Tejada, P. J., Rueda, C. A., & Ustin, S. L. (2003). Water content estimation in vegetation with MODIS reflectance data and model inversion methods. *Remote Sensing of Environment*, *85*, 109−124.

Zha, Y., Gao, J., & Ni, S. (2003). Use of normalized difference built-up index in automatically mapping urban areas from TM imagery. *International Journal of Remote Sensing*, *24*(3), 583−594.

Zhao, H. M., & Chen, X. L. (2005). Use of normalized difference bareness index in quickly mapping bare areas from TM/ETM+. *Geoscience and Remote Sensing Symposium*, *3*(25–29), 1666−1668.

Zhong, B. (1996). Urban heat island effect of Shenzhen city. *Journal of Meteorology*, *22*(5), 23−24.